

Coherence Transfer and Destructive Interference in Two-Dimensional Coherence Maps

Amitav Sahu¹ and Vivek Tiwari ^{*1}

¹Solid State and Structural Chemistry Unit, Indian Institute of Science, Bangalore,
Karnataka 560012, India

February 2, 2023

Abstract

Coherence maps (CMs) in multidimensional spectroscopy report total interference of all quantum coherent pathways. Detailed understanding of how this interference manifests spectroscopically is vital for deciphering mechanistic origins of impulsively generated wavepackets, but currently lacking. Here we explain the origin of recently reported diagonal node-like features in CMs of *bacteriochlorophyll* monomers and photosynthetic reaction centers (RCs), where the apparent resemblance in the two disparate systems was reportedly perplexing. We show that both spectroscopic signatures have distinct physical origins. Node-like lineshapes in monomers arise from unique phase twists caused by destructive interference between ground and excited state vibrational coherences. In contrast, nodal lines in RCs are explained by coherence transfer of vibrational wavepackets which do not participate in the ultrafast energy transfer and their destructive interference with ground state pathways. Our results resolve recent spectroscopic observations and illustrate new mechanistic insights gained from understanding interference effects in multidimensional spectroscopy.

Two-dimensional electronic spectroscopy¹ (2DES) resolves ultrafast dynamics ensuing femtosecond excitation as 2D contour map snapshots along initially correlated excitation and detection frequency axes, evolving along the pump-probe waiting time T . Analysis of coherent signal contributions, often accompanying impulsive excitations, along the corresponding frequency axis ω_T leads to coherence maps (CMs). At a given ω_T , CMs report the total interference of all quantum coherent Feynman pathways which may arise from distinct origins, for instance, from purely vibrational versus mixed vibrational-electronic wavepackets, or from wavepackets on ground versus excited electronic states.

*vivektiwari@iisc.ac.in

CM analysis of peak positions² can disentangle overlapping signal contributions with varying degree of success, and despite spectral decongestion along three dimensions, ambiguous spectroscopic signatures can still arise. For example, recent 2DES experiments on photosynthetic reaction centers (RCs) have reported^{3,4} diagonal nodes in CMs for all reported intramolecular vibrational frequencies. However similar diagonal node-like interference effects were later reported⁵ in CMs of bacteriochlorophyll (*BChl a*) monomers. These similarities in spectroscopic signatures from multichromophoric RCs and *BChl a* monomers in solution were reportedly perplexing. Here we show that these apparently similar spectroscopic signatures arise from distinct physical mechanisms, and illustrate how CM lineshapes serve as subtle reporters of the underlying physics of vibrational coherence transfer^{6,7} and destructive interference between signal pathways contributing to 2D spectra.

To address the above questions, we start by deriving analytic expressions for CM lineshapes to show that uniquely different phase-twists, as opposed to those arising from imbalanced rephasing and non-rephasing signals, can arise due to interference between Feynman pathways for ground and excited vibrational wavepackets. We will show that reported⁵ diagonal node-like features in 2DES CMs of *BChl a* monomers are manifestations of this interference. We consider the simplest model of a three electronic level system with a Franck-Condon (FC) active intramolecular vibration identically coupled to all three electronic states. Note that unlike the transition strengths derived from 2-electrons in a 2D box model for D_{4h} symmetric monomers, only one-electron transition strengths are expected⁸ in *BChl a* due large electronic splitting between the Q_x and Q_y bands. The ground state bleach (GSB), excited state emission (ESE) and absorption (ESA) Feynman pathways for vibrational quantum coherences that contribute to the 2DES diagonal peak (DP) can be written as a product of an orientational factor arising from four transition dipole factors interacting with the pump and probe electric fields, and a Green's function time-propagator $\mathcal{G}(t)$ for each time interval between light-matter interactions. The GSB, ESE and ESA rephasing Feynman pathways for vibrational coherences on the 2D diagonal are given by Eqns. S1–S3 and represented as wavemixing diagrams in Fig. 1B and Fig. S1.

Only dominant 0–1 vibrational coherences and Bloch dephasing have been considered in Eqns. S1–S3 for the purpose of deriving analytic expressions. In the Bloch limit, $\mathcal{G}_{mn}(t) = \theta(t)\exp[-\gamma_{mn}(t)]\exp[-i\omega_{mn}t]$, where $\theta(t)$ is the Heaviside step function, $\omega_{mn} = (E_m - E_n)/\hbar$, and γ_{mn} is the dephasing rate. It is reasonable to expect ground and excited state vibrational coherences to dephase with different rates along T , denoted by γ_g and γ_e , respectively. Optical Bloch dephasing rates have been assumed to be equal for simplicity, and denoted by γ . Note that the 2D lineshape is determined by the product of Green functions, while the transition dipoles impart an overall strength and sign. All such individual lineshapes interfere to result in total 2D signal strength and lineshape. Crucially, sign of the coherence frequency along T is opposite for GSB versus ESE and ESA pathways (Fig. S1), and dictates the diagonal node-like interference feature as explained below.

Inverse Fourier transformation of Eqns. S1-S3 along the first and third time intervals yields 2D lineshapes along excitation and detection frequencies, $-\omega_\tau$ and ω_t , for each non-zero value of waiting time T . For the case of GSB pathways, the resulting frequency domain complex 2D signal \tilde{S}_3 is given by –

$$\begin{aligned}\tilde{S}_3(-\omega_\tau, \omega_t; T) &= \mathcal{F}^{-1}[\mathcal{G}_{g_0e_0}(\tau)]\mathcal{G}_{g_0g_1}(T)\mathcal{F}^{-1}[\mathcal{G}_{e_1g_1}(t)] \\ &= [\alpha(-\omega_\tau, \omega_t) - i\beta(-\omega_\tau, \omega_t)]e^{-i\omega_v T}e^{-\gamma_g T},\end{aligned}\quad (1)$$

where vibrational coherence frequency along T has been substituted by the vibrational frequency ω_v . $a_{mn}(\omega)$ and $d_{mn}(\omega)$ are absorptive and dispersive 2D Lorentzian lineshapes, respectively, with

$$\begin{aligned}\alpha(-\omega_\tau, \omega_t) &= [a_{g_0e_0}(-\omega_\tau)a_{e_1g_1}(\omega_t) - d_{g_0e_0}(-\omega_\tau)d_{e_1g_1}(\omega_t)] \\ \beta(-\omega_\tau, \omega_t) &= [a_{g_0e_0}(-\omega_\tau)d_{e_1g_1}(\omega_t) + a_{e_1g_1}(\omega_t)d_{g_0e_0}(-\omega_\tau)]\end{aligned}\quad (2)$$

In the same fashion, including the ESE and ESA contributions, the total complex 2D signal becomes –

$$\tilde{S}_{tot}(-\omega_\tau, \omega_t; T) = [\alpha(-\omega_\tau, \omega_t) - i\beta(-\omega_\tau, \omega_t)](e^{i\omega_v T}e^{-\gamma_e T}(1 - \kappa) + e^{-i\omega_v T}e^{-\gamma_g T}).\quad (3)$$

where an ESA strength factor κ has been included to account for any differences in transition strengths of doubly-excited states. See Section S1 for details of the derivation. To derive CM lineshapes from a real rephasing 2D spectrum $S_{tot}^R(-\omega_\tau, \omega_t; T)$, we will consider special cases of Eqn. 3. Experimental absorptive 2D spectra of *BChl a* monomers have reported⁵ very weak off-diagonal contributions from excited state absorption (ESA) with negligible contribution on the 2D diagonal. Accordingly we simplify Eqn. 3 to first consider only excited state emission (ESE) and ground state bleach (GSB) pathways with κ set to zero. Assuming dephasing rates of excited and ground state vibrational coherences such that $\gamma_e \approx \gamma_g = \gamma_{g,e}$, and Fourier transforming along T yields the corresponding CM lineshape contributing on the diagonal with frequency $\omega_T = \omega_v$, $CM_{tot}(-\omega_\tau, \omega_t; \omega_T) = \text{abs}[\alpha(-\omega_\tau, \omega_t)a(\omega_T = \omega_v)]$, where the absolute value is consistent with how 2DES CMs are typically reported. Inspection of the CM lineshape $CM_{tot}(-\omega_\tau, \omega_t; \omega_T)$ suggests reduction in diagonal amplitude due to cancellations between $a(-\omega_\tau)a(\omega_t)$ and $d(-\omega_\tau)d(\omega_t)$ terms in $\alpha(-\omega_\tau, \omega_t)$ (Eqn. 3). Although the latter term vanishes at the peak center, it removes amplitude from off-center locations above and below the diagonal. This destructive interference between ESE and GSB coherence pathways on the DP is distinct from the phase-twist quantum beats arising⁹ from imbalance between rephasing and non-rephasing pathways. The GSB/ESE destructive interference discussed here only arises at the DP and not on other 2D CM locations (see Fig. S2) because opposite phases of vibrational quantum coherences only overlap on the

diagonal (Eqn. 2). 2DES simulations with Bloch lineshapes confirm the narrowed diagonal lineshapes in CMs arising from destructive interference between GSB/ESE vibrational coherence pathways. These are shown in Section S1.

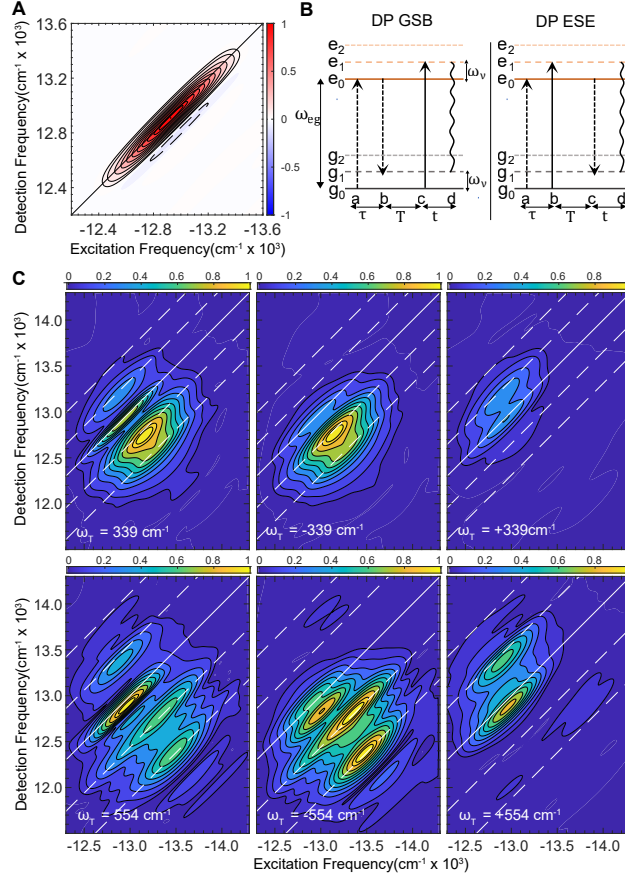


Figure 1: (A) Real absorptive $T = 50$ fs 2D spectrum of a two electronic level system with five underdamped FC vibrations modeled as Brownian oscillators to simulate coherence maps (CMs) for dominant vibrational coherences recently reported⁵ in *Bacteriochlorophyll a* monomer. The spectrum is calculated at 77 K. The model parameters are described in Table S2. Contours are drawn at the 5%, and 10-90% in 10% intervals for positive or negative contours. (B) Wavemixing diagrams corresponding to 2DES signal contributions at the diagonal peak arising from ground (GSB) and excited state (ESE) vibrational coherences. (C) Real rephasing (left) and $-\omega_T$ (center) and $+\omega_T$ (right) complex rephasing CMs for vibrational frequencies 339 cm⁻¹ and 554 cm⁻¹. CMs at other vibrational frequencies are shown in Fig. S4. The narrowing of diagonal CM lineshape in the real rephasing CMs due to the destructive interference between overlapping GSB and ESE coherent pathways of panel B is evident for all vibrational coherences in the model.

We extend the above analytic reasoning to simulate the recently reported 2D CMs of *BChl a* monomers at 77K. The model parameters are described in Section S2. Briefly, the reported FC active intramolecular vibrations are modeled as underdamped Brownian oscillators with stabilization energies, damping and frequencies similar to those reported for *BChl a* monomers.^{5,10,11} Energetic disorder of 230 cm⁻¹ in the optical energy gap is also included in the model to approximately match the diagonal linewidth reported⁵ for early T 2DES spectra of *BChl a* monomers. All the simulation parameters are summarized in Table S2. Figure 1A shows the $T = 50$ fs absorptive 2DES spectrum. A Frobenius spectrum of vibrational coherences corresponding to all intramolecular vibrations in the model is shown in Fig. S3. Fig. 1B shows the GSB and ESE wavemixing diagrams which interfere on the 2D diagonal. The real rephasing CMs for two of the intramolecular vibrations are shown in the left column of Fig. 1C. Rest

of the CMs are shown in Fig. S4. As expected, for all vibrations, the $d_{g_0e_0}(-\omega_\tau)d_{e_1g_1}(\omega_t)$ term in $CM_{tot}(-\omega_\tau, \omega_t; \omega_T)$, that results from the interference of GSB and ESE vibrational coherence pathways, leads to narrow node-like features on the 2D diagonal. Compared to simulations with Bloch lineshapes (Fig. S2), these features are further accentuated by energetic disorder in the optical energy gap in the reported⁵ 2D spectra at 80K. It can be easily verified that when one starts from the complex rephasing 2D spectrum $\tilde{S}_{tot}(-\omega_\tau, \omega_t; T)$ (Eqn. 3), the absolute value CM lineshape for the case of $\omega_T = \pm\omega_v$ is now given by $\mathcal{R}(-\omega_\tau, \omega_t) = \sqrt{\alpha^2(-\omega_\tau, \omega_t; T) + \beta^2(-\omega_\tau, \omega_t; T)}$, which does not predict a diagonal narrowing but instead an approximately absorptive lineshape. It is therefore no surprise that when the CMs are resolved according to the quantum beat phase $\pm\omega_T$ (Fig. 1C middle and right panels), DP narrowing due to GSB/ESE destructive interference does not occur. Note that the above reasoning suggests that the diagonal node-like feature is not specific to *BChl a*. Recent real rephasing CMs for Oxazine 720 monomers¹² are consistent with this expectation.

In deriving $CM_{tot}(-\omega_\tau, \omega_t; \omega_T)$ lineshape it is assumed that the dephasing timescale of excited and ground state vibrational coherences is comparable, that is, $\gamma_g \sim \gamma_e$. However, ultrafast electronic relaxation channels can cause large anharmonicities on the excited state potentials such that some excited state vibrational wavepackets may not survive electronic relaxation.^{13,14} For example, vibrational quantum beats from ‘promoter’ modes¹⁵ that *tune* the relative energy gaps and electronic couplings between excited state potentials do not survive relaxation through a conical intersection and dephase¹⁶ within ~ 100 fs. In contrast, the ground state beats survive for picoseconds. The above assumption will also be invalidated in systems exhibiting ultrafast singlet exciton fission, such as pentacene thin films, due to rapid internal conversion¹⁷ of excited state population into correlated triplet states. In all such cases, Eqn. 3 predicts absence of diagonal node-like GSB/ESE interference feature in the CMs.

Interestingly, the CM lineshape then also becomes a useful spectroscopic reporter of ‘promoter’ vibrational modes and excited state dynamics. For example, Policht et al. reported⁵ no change in the diagonal node-like feature for *BChl a* for penta- or hexa-coordinating solvents, suggesting no substantial effect on the dephasing rates of ground and excited vibrational wavepackets due to solvent coordination. Recent broadband pump-probe measurements from Scholes and coworkers report that solvent tuning of electron transfer rates can dephase¹⁸ vibrational modes parallel to the reaction coordinate up to 5x faster, whereas ‘spectator’ modes remain unaffected. Our analysis of GSB/ESE interference predicts that in a corresponding 2DES experiment, as opposed to ‘spectator’ modes, the diagonal CM lineshapes for ‘promoter’ modes will *not* show the node-like diagonal lineshape.

Having explained the node-like features reported for *BChl a* monomers, we can now investigate similar spectroscopic signatures that were reported^{3,19} to accompany ultrafast energy transfer in bacterial RC proteins (BRCs). Recently, Zigmantas and co-workers reported³ diagonal nodes in all the vibrational

CMs from a chemically oxidized BRC undergoing sub-200 fs $H \rightarrow B$ energy transfer. Interestingly, similar nodes are also reported by Ogilvie and co-workers^{4,19} in the context of $B \rightarrow P$ energy transfer for mutant BRCs, even when charge separation is precluded²⁰ (D_{LL} mutant). Similarities in diagonal nodes for the two cases are curious. Furthermore, in all above cases, dominant ESA contributions on the upper diagonal 2D peak (DP_U) are also reported. Bukarté et al. have explained²¹ these contributions using ESA related "re-excitation" Feynman pathways with dispersive lineshapes caused by electrochromic shifts induced when charge separation is complete at long waiting times pump-probe ($T > 2$ ps). However, dispersive lineshapes are seen²⁰ for as early as 250 fs, and even for the D_{LL} mutant. For example, see Fig. S2 and Fig. S6 of ref.²⁰.

Paleček et al.³ have qualitatively argued for an excited to ground state coherence shift explain the nodal feature. Recent experiments, supported by simulations, from Policht et al.¹⁹ explain coherent ESA contributions in the upper 2D cross-peak region by incorporating a distinctly different coherence transfer mechanism between excited state vibronic eigenstates. Overall, presence of nodal lines on the diagonal for all reported intramolecular vibrations, even for BRC mutants incapable of charge separation, and the similarity with node-like diagonal features in *BChl a* monomers⁵ has remained perplexing and begs further explanation. While destructive GSB/ESE interference (Fig. 1) already explains the diagonal node-like CM lineshapes in monomers, below we explain the distinct physical origin for the reported diagonal nodal lines.

We consider an excitonic dimer model with two intramolecular FC vibrations, as a minimum model for $P - B$ or $B - H$ exciton pairs studied earlier.^{3,19} The rapid energy transfer process is complete within ~ 200 fs and the reported CMs correspond to vibrational wavepackets which survive energy transfer. In order to incorporate electronic relaxation in wavemixing pathways, we adopt the recently reported²² approach of Engel and co-workers which exploits symmetries between 2D diagonal and cross peaks (as they grow or decay due to electronic relaxation) to extract population transfer kinetics. In the context of coherence transfer accompanying ultrafast electronic relaxation, multilevel Redfield simulations⁶ of Jean and Fleming are quite instructive. Their results suggest that coherent vibrational motions orthogonal to the 'reaction coordinate' can undergo coherence transfer to the acceptor through dominant secular terms in the Redfield tensor, $\mathbf{R}_{\alpha\beta,\gamma\delta}$ as long as the coherence frequency is maintained on the donor and acceptor excitons, that is, $\omega_{\alpha\beta} = \omega_{\gamma\delta}$, respectively. This is so because orthogonal spectator motions maintain the donor-acceptor energy gap, while energy gap tuning motions lead to 'nesting'¹⁴ of donor-acceptor electronic states and may not survive energy transfer. Witkowskii and Moffitt,²³ and later others^{24,25} have analyzed donor-acceptor energy transfer in terms of symmetric or correlated \hat{q}_+ and anti-symmetric or anti-correlated \hat{q}_- , relative motions of intramolecular vibrational coordinates $\hat{q}_{A,B}$ on

the respective molecules. Using a surface-crossing description of electronically coherent donor-acceptor energy transfer, Cina and Fleming⁷ have elucidated the interplay of vibrational coherence transfer and in-phase or symmetric vibrational motions between the donor and acceptor. Correlated vibrations play the role of spectator motions in an excitonic dimer. Since they maintain donor-acceptor energy gap, coherence transfer is expected to be dominant along correlated modes.

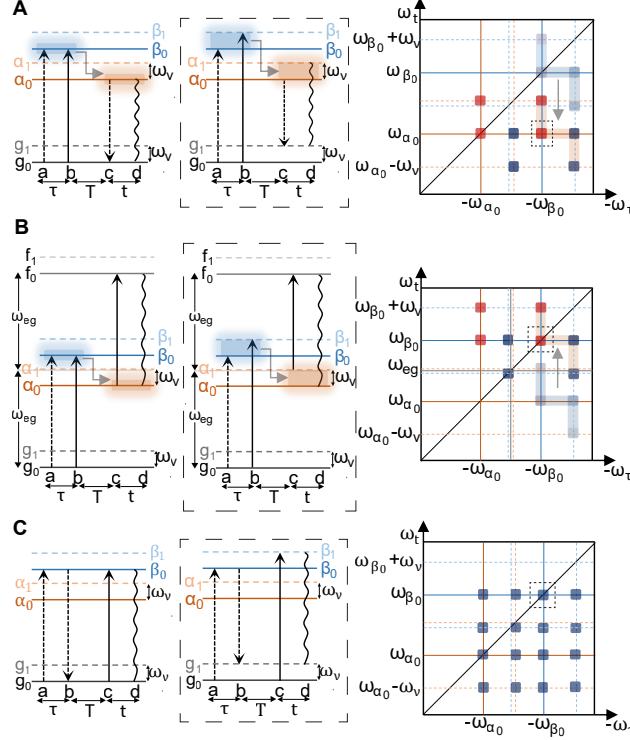


Figure 2: Wavemixing pathways with electronic relaxation through population and coherence transfer. (A) ESE wavemixing pathway corresponding to (left) population relaxation and (middle) vibrational coherence transfer from the donor β to acceptor α excitons. (right) Expected 2D CM locations of 0-1 vibrational coherences arising from real rephasing ESE pathways. Red and blue squares denote the quantum beat phase $+\omega_T$ and $-\omega_T$, respectively. Subscripts 0,1 denote vibrational levels separated by frequency ω_v . Length of first and last arrow in the wavemixing pathways determines the 2D location along the excitation and detection axis, respectively. The arrow marks the chair shift from DP_U to CP_L due to vibrational coherence transfer. The wavemixing diagram for the peak highlighted by the dashed square is shown in the middle figure, all other pathways are shown in Fig. S6. (B) ESA wavemixing pathways and CM contributions. The CM chair shifts opposite to ESE, from CP_L to DP_U (C) GSB wavemixing pathways and CM contributions. From the 2D CMs, it is evident that after vibrational coherence transfer, CM contributions on DP_U will be a result of interfering GSB and ESA pathways.

Fig. 2 connects wavemixing diagrams incorporating ultrafast $D \rightarrow A$ population relaxation and vibrational coherence transfer to corresponding contributions on the 2D spectrum. It is well understood²² that the 2D locations of ESE and ESA population contributions on DP_U and lower cross-peak (CP_L), respectively, will be interchanged by population transfer. This is illustrated in the wavemixing pathways in the first column in Figs. 2A-C. However, it is vital to recognize the corresponding evolution of coherence pathways after vibrational coherence transfer. This is shown in the wavemixing pathways in the middle column, with corresponding 2D CM contributions in the right column. Interestingly, due to vibrational coherence transfer dominant along spectator modes such as \hat{q}_+ in an excitonic dimer, a concomitant shift in the positions of coherence peaks is also expected. 0-1 vibrational coherences contribute as a chair

pattern²⁶ in a 2D CM, such that the entire chair pattern of ESE/ESA coherence peaks is interchanged as well. Only wavemixing pathways for one of the coherence peaks is shown and marked as dashed square in the 2D CM. All other contributions are shown in Fig. S6. Recalling monomer CM lineshapes in Eqns. 2–3, vibrational coherence transfer in an excitonic dimer implies ESE vibrational coherence pathways on DP_U are replaced by ESA, which interfere with unshifted GSB pathways to result in $\beta(-\omega_\tau, \omega_t)$ nodal lineshapes, with the extent of destructive interference on the 2D diagonal dependent on ESA strength κ .

In order to confirm the above expectations, we simulate 2DES spectra which include exact non-adiabatic couplings through numerically diagonalized eigenvectors, phenomenological population relaxation and coherence transfer through phenomenological relaxation incorporated in sum-over-states response functions,²⁷ optical decoherence through Brownian oscillators and ensemble dephasing¹³ of vibronic coherences through energetic averaging. The vibrational frequencies and weak FC displacements are based on intramolecular FC active vibrations of *BChl a*. In the study of Paleček et al.,³ the $B - H$ exciton energy gap of 650 cm^{-1} was in vibronic resonance²⁸ with a prominent intramolecular vibrational frequency of *BChl a*. Enhanced²⁸ GSB vibrational coherences arising from this resonance were previously reported²⁹ by Ryu et al. To study the effect of vibronic resonance on the expected destructive interference, the diabatic exciton energy gap is chosen to be resonant with a 650 cm^{-1} intramolecular vibration, while the other vibrational frequency of 350 cm^{-1} does not participate in resonant vibronic mixing. Choosing a resonant and non-resonant vibrational mode provides a minimum model to explain the diagonal nodal lines reported^{3,19} for *all* observed intramolecular vibrations. Note that we choose complete two-particle basis sets in our calculations such that vibronic enhancement and multiple wavemixing pathways³⁰ due to resonance are accurately captured in the simulations. Describing multiple wavemixing pathways arising at resonance is necessary to assess whether they appreciably perturb the destructive interference on the 2D diagonal. The anti-correlated energetic disorder of 68 cm^{-1} is chosen such that ensemble dephasing¹³ of purely electronic coherences is complete within $\sim 200 \text{ fs}$ and consistent with experiments.³

Following previous approaches^{19,31} treating vibrational coherence transfer phenomenologically through Feynman pathways, the model here does not consider the details of ultrafast energy transfer mechanism. Instead population transfer timescale of $\sim 50 \text{ fs}$ ^{20,32} is included phenomenologically, such that the energy transfer is near complete³ by $\sim 200 \text{ fs}$. $\mathbf{R}_{\alpha\beta=\gamma\delta}$ coherence transfer is also included phenomenologically in the analytic response functions (Section S3). The simulations are carried out in the site basis with intramolecular vibrational coordinates $\hat{q}_{A,B}$ which allow for both correlated \hat{q}_+ and anti-correlated \hat{q}_- vibrational motions on the donor and acceptor excitons. To understand whether vibronic resonance affects the diagonal nodal line, calculations along only the spectator mode \hat{q}_+ where no resonant vibronic mixing is possible,³³ are also analyzed. Vibronic coherences are not expected to survive anharmonic non-adiabatic couplings.³⁴ Experimentally, dephasing rates for such wavepackets are not known in case

of RCs. For a photosynthetic antenna, Thyrgaug et al. have reported² $\sim 4\text{-}5\times$ faster dephasing of vibronic versus purely vibrational wavepackets. In our simulations, we do not include any excited state dephasing for vibronic wavepackets. This allows us to infer the effect of surviving vibronic coherences, if any, on the expected nodal line.

Because symmetric vibrations in an excitonic dimer maintain a fixed donor-acceptor energy gap, they do not participate²⁸ in vibronic mixing, such that, in the simulations, vibronic eigenvectors with \hat{q}_+ excitations undergo vibrational coherence transfer. In contrast, vibronic eigenvectors with only \hat{q}_- excitations strongly mix excitons near a vibronic resonance to result in energetic splittings (for example, see Fig. 1 of ref.³⁵). Consequently, the corresponding vibronic wavepackets in the simulations do not undergo coherence transfer. A multiplicative factor κ is included in the ESA response as a parameter to account for the collective ESA transition strength. Fig. S2 and Fig. S6 of ref.²⁰ suggest that ESA contributions on the main diagonal peak are already significant by $T = 250$ fs. Similar to experiments, the CMs are calculated from $T = 200$ fs after dephasing of electronic coherence and energy transfer are approximately complete. All the model parameters are described in Section S3.

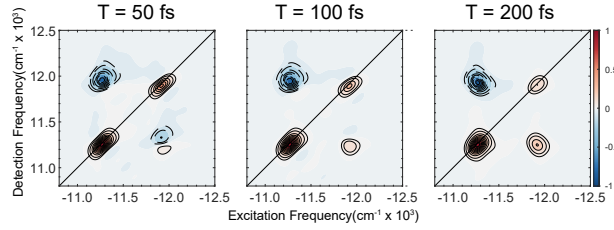


Figure 3: Real absorptive 2D spectra for waiting times $T = 50, 100$ and 200 fs with an ESA signal strength of $\kappa = 2$ and temperature of 77 K. The simulations details and model parameters are described in Section S3.

Fig. 3 shows the total absorptive 2D spectra at $T = 50, 100$ and 200 fs using the above model. As expected from the analysis in Fig. 2, population relaxation between excitons causes DP_U and CP_L ESE population signals to decay and grow, respectively, with an opposite trend for ESA signals. The total 2D signal at DP_U is diminished due to the cancellation of positive GSB and negative ESA signals with increasing waiting time T , consistent with experiments which report²⁰ a dominant ESA signal on DP_U . The corresponding 2D CMs are shown in Fig. 4 for the resonant 650 cm^{-1} and the non-resonant 350 cm^{-1} vibration. The CMs are zoomed in on DP_U to highlight the expected destructive interference on the 2D diagonal due to vibrational coherence transfer along the spectator modes. Zoomed out CMs are shown in Figs. S7–S8. Fig. 4A compares the DP_U diagonal node for a resonant versus non-resonant vibration. The calculation assumes that excited state vibronic wavepackets along the tuning mode \hat{q}_- survive energy transfer. Both vibrations show a nodal line on DP_U due to GSB-ESA destructive interference. However, the destructive interference for the resonant vibration is strongly perturbed by unshifted ESE vibronic coherence contributions due to lack of coherence transfer along \hat{q}_- . This is accentuated further

by multiple wavemixing pathways contributing on DP_U at resonance (Section S5). In contrast, Fig. 4B shows a calculation only along the spectator mode \hat{q}_+ which does not participate²⁸ in vibronic mixing. As expected, a clean nodal line consistent with experimental reports is seen on DP_U due to destructive interference of GSB-ESA coherent pathways following vibrational coherence transfer. These findings suggest that vibronic wavepackets either do not survive energy transfer or there is only weak resonant vibronic mixing in case of BRCs due to sub-peaks within the B and H bands in BRCs³⁶ and narrow vibronic resonance widths.^{33,35} The former seems plausible given the recent observations² of Thyrgaugh et al. of ~ 4 - 5 x faster dephasing of vibronic versus vibrational wavepackets in a photosynthetic antenna. The last two rows in Fig. 4B show that, as expected, when CMs are resolved according to quantum beat phase along ω_T , destructive interference on the 2D diagonal does not occur. Note that the impulsive 2D calculation presented here allows all CM peaks to be prominent. Laser pulse frequency filter²⁷ from a finite pulse is expected to suppress off-diagonal CM peaks. The above model and calculations have assumed perpendicular and equal magnitude excitonic transition dipoles to preclude any transition dipole interference effects. However, transition dipoles in RCs are not perpendicular or of equal magnitude. Below we consider whether interference between non-orthogonal unequal magnitude transition dipoles in RCs can cause nodal line feature to appear readily. We have derived an analytic expression for ESA strength κ required for complete destructive interference on DP_U , as a function of excitonic transition dipole angle $\theta_{\alpha\beta}$ and their relative oscillator strength ratio m . The derivation is described in Section S4, with final expression given by,

$$\kappa = \frac{3m}{1 + 2 \cos^2(\theta_{\alpha\beta})}, \quad (4)$$

and plotted in Fig. 4C. An ESA strength of $\kappa = 3$ is required for complete destructive interference in case of perpendicular and equal magnitude transition dipoles. Table S4 calculates the transition dipole strengths and directions expected^{32,37} from P , B and H excitons in the BRCs. Using Eqn. 4 and Table S4, in case of BRCs the ESA strength required for GSB-ESA destructive interference is reduced to $\kappa \sim 2$ for both $P - B$ and $B - H$ exciton pairs. This seems reasonable as a collective ESA strength given the multiple two-quantum electronic manifolds in the RCs and the experimental observations (Fig. S2 and Fig. S6 of ref.²⁰). Fig. S10 compares the nodal feature in Fig. 4B for ESA strengths of $\kappa = 1$ - 3 . The insensitivity of destructive interference to κ suggests that the nodal feature, although imbalanced, is expected to be persistent over a range of ESA strengths. Several additional effects such as peak overlaps, inhomogeneous broadening, laser pulse filter, and red- or blue-shifted ESA signals due to electrochromic shifts can also cause an imbalanced nodal feature. For example, Fig. S11 shows that DP_U node becomes imbalanced, although persistent, even when expected²¹ BRC electrochromic shift of ~ 100 - 200 cm^{-1} is included.

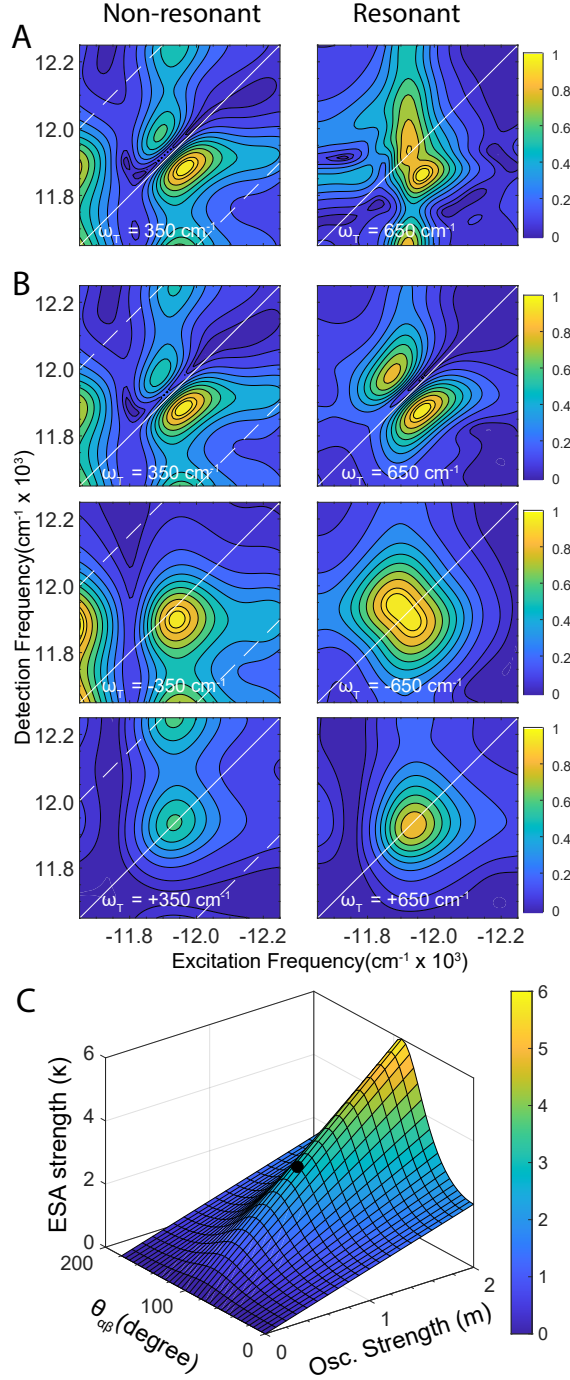


Figure 4: (A) Zoomed DP_U real rephasing 2D CM for non-resonant (350 cm^{-1}) and resonant (650 cm^{-1}) vibration. The calculation corresponds to the case where both \hat{q}_- and \hat{q}_+ tuning and spectator modes, respectively, are allowed. (B) 2D CM calculation with only spectator mode \hat{q}_+ (top), and resolved into $-\omega_T$ (middle) and $+\omega_T$ (bottom) components. The full CMs with the red square around DP_U are shown in Figs. S7–S8. Contours are drawn at the 5%, and 10–90% in 10% intervals. (C) The surface plot of ESA signal strength κ required for complete destructive interference between GSB-ESA coherence pathways, as a function of the relative excitonic oscillator strength (m) and the angle between the excitonic transition dipoles ($\theta_{\alpha\beta}$). The detailed strength calculation is shown in Section S4. Black dot shows required κ for perpendicular and equal magnitude transition dipoles.

Coherence transfer along spectator modes is expected to accompany ultrafast electronic energy transfer. Our simulations of excitonic dimer model and Feynman pathways account for this phenomenologically without considering the details of energy transfer or multiple 1- and 2-quantum electronic manifolds

in the RCs. This phenomenological treatment of coherence transfer between vibronic eigenstates is consistent with that recently proposed by Policht et al.¹⁹ to explain coherence contributions in the upper cross-peak region arising from ESA pathways. In our case, by accounting for shifting population and coherence contributions in the 2D spectra, we have shown that the resulting GSB-ESA interference between coherent pathways contributing on the 2D diagonal produces persistent signatures, similar to those reported in BRC 2DES studies²⁰ for all observed intramolecular vibrations.

Conclusions

Our results provide new insights on the connections between vibrational coherence transfer, interference between coherent Feynman pathways and the resulting 2D CM lineshapes. By establishing these connections we resolve the distinct physical origins that lead to reportedly³⁻⁵ similar nodal diagonal lineshapes in the 2D CMs of two disparate systems, *BChl a* monomer and multichromophoric BRCs. We show that while the former arises from unique phase-twists from interfering GSB-ESE coherence pathways, the latter is fundamentally different and arises from previously overlooked vibrational coherence transfer along spectator modes accompanying ultrafast electronic relaxation. By incorporating relaxation pathways in Feynman diagrams, we show that along with population transfer, vibrational coherence transfer leads to a concomitant shift of coherence contributions on the 2D CM spectrum. Such coherence-shifts are expected to be dominant along spectator modes. The resulting destructive interference between GSB-ESA signal pathways is consistent with the reported nodal lines on the 2D diagonal. From experimental observations of dominant ESA signals, and estimations of dipole strengths and directions in BRCs, our analysis suggests that such nodal lines may be readily expected in BRCs. Our results resolve recent spectroscopic observations, highlight the rich information content of a 2D CM spectrum, and establish its usefulness as a subtle spectroscopic reporter of underlying electronic relaxation mechanisms.

Acknowledgments

AS acknowledges research fellowship from the Indian Institute of Science (IISc). This project is supported by Science and Engineering Research Board, India under grant sanction number CRG/2019/003691 and Department of Biotechnology, India under grant sanction number BT/PR38464/BRB/10/1893/2020.

Supporting Information Available

Bloch model analytical calculations, monomer 2D simulation parameters, 2D simulations with population and coherence transfer, simulations for ESA strength dependence of nodal line, multiple sub-peaks on upper 2D diagonal at vibronic resonance, analytical expression for nodal line with generalized transition

dipole directions and magnitudes, 2D and CM calculations with blue shifted ESA signal, Figures S1–S11.

References

- [1] Jonas, D. M. Two-Dimensional Femtosecond Spectroscopy. *Annu. Rev. Phys. Chem.* **2003**, *54*, 425–463.
- [2] Thyryhaug, E.; Tempelaar, R.; Alcocer, M. J. P.; Židek, K.; Bina, D.; Knoester, J.; Jansen, T. L. C.; Zigmantas, D. Identification and characterization of diverse coherences in the Fenna–Matthews–Olson complex. *Nature Chemistry* **2018**, *10*, 780–786.
- [3] Paleček, D.; Edlund, P.; Westenhoff, S.; Zigmantas, D. Quantum coherence as a witness of vibronically hot energy transfer in bacterial reaction center. *Science Advances* **2017**, *3*.
- [4] Policht, V. Observations of Coherence in Bacterial Reaction Centers Using Two-Dimensional Electronic Spectroscopy. Ph.D. thesis, University of Michigan, Ann Arbor, 2018.
- [5] Policht, V. R.; Niedringhaus, A.; Ogilvie, J. P. Characterization of Vibrational Coherence in Monomeric Bacteriochlorophyll a by Two-Dimensional Electronic Spectroscopy. *The Journal of Physical Chemistry Letters* **2018**, *9*, 6631–6637.
- [6] Jean, J. M.; Fleming, G. R. Competition between energy and phase relaxation in electronic curve crossing processes. *The Journal of Chemical Physics* **1995**, *103*, 2092–2101.
- [7] Cina, J. A.; Fleming, G. R. Vibrational Coherence Transfer and Trapping as Sources for Long-Lived Quantum Beats in Polarized Emission from Energy Transfer Complexes. *The Journal of Physical Chemistry A* **2004**, *108*, 11196–11208.
- [8] Weiss, C. The π electron structure and absorption spectra of chlorophylls in solution. *Journal of Molecular Spectroscopy* **1972**, *44*, 37–80.
- [9] Cho, B.; Yetzbacher, M. K.; Kitney, K. A.; Smith, E. R.; Jonas, D. M. Propagation and Beam Geometry Effects on Two-Dimensional Fourier Transform Spectra of Multilevel Systems. *The Journal of Physical Chemistry A* **2009**, *113*, 13287–13299.
- [10] Rätsep, M.; Cai, Z.-l.; Reimers, J. R.; Freiberg, A. Demonstration and interpretation of significant asymmetry in the low-resolution and high-resolution Q y fluorescence and absorption spectra of bacteriochlorophyll a. *J. Chem. Phys.* **2014**, *024506*.
- [11] Wendling, M.; Pullerits, T.; Przyjalowski, M. A.; Vulto, S. I. E.; Aartsma, T. J.; van Grondelle, R.; van Amerongen, H. Electron-Vibrational Coupling in the Fenna-Matthews-Olson Complex of Pros-

- thecochloris aestuarii Determined by Temperature-Dependent Absorption and Fluorescence Line-Narrowing Measurements. *The Journal of Physical Chemistry B* **2000**, *104*, 5825–5831.
- [12] Sahu, A.; Bhat, V. N.; Patra, S.; Tiwari, V. High-sensitivity fluorescence-detected multidimensional electronic spectroscopy through continuous pump–probe delay scan. *The Journal of Chemical Physics* **2023**, *158*, 24201.
- [13] Jonas, D. M. Vibrational and Nonadiabatic Coherence in 2D Electronic Spectroscopy, the Jahn–Teller Effect, and Energy Transfer. *Annual Review of Physical Chemistry* **2018**, *69*, 327–352.
- [14] Rafiq, S.; Scholes, G. D. From Fundamental Theories to Quantum Coherences in Electron Transfer. *Journal of the American Chemical Society* **2019**, *141*, 708–722.
- [15] Patra, S.; Sahu, A.; Tiwari, V. Effective normal modes identify vibrational motions which maximally promote vibronic mixing in excitonically coupled aggregates. *The Journal of Chemical Physics* **2021**, *154*, 111106.
- [16] Farrow, D. A.; Qian, W.; Smith, E. R.; Ferro, A. A.; Jonas, D. M. Polarized pump-probe measurements of electronic motion via a conical intersection. *The Journal of Chemical Physics* **2008**, *128*, 144510.
- [17] Wilson, M. W. B.; Rao, A.; Clark, J.; Kumar, R. S. S.; Brida, D.; Cerullo, G.; Friend, R. H. Ultrafast Dynamics of Exciton Fission in Polycrystalline Pentacene. **2011**, 11830–11833.
- [18] Yoneda, Y.; Kudisch, B.; Rafiq, S.; Maiuri, M.; Nagasawa, Y.; Scholes, G. D.; Miyasaka, H. Vibrational Dephasing along the Reaction Coordinate of an Electron Transfer Reaction. *Journal of the American Chemical Society* **2021**, *143*, 14511–14522.
- [19] Policht, V. R.; Niedringhaus, A.; Willow, R.; Laible, P. D.; Bocian, D. F.; Kirmaier, C.; Holten, D.; Mančal, T.; Ogilvie, J. P. Hidden vibronic and excitonic structure and vibronic coherence transfer in the bacterial reaction center. *Science Advances* **2022**, *8*, eabk0953.
- [20] Niedringhaus, A.; Policht, V. R.; Sechrist, R.; Konar, A.; Laible, P. D.; Bocian, D. F.; Holten, D.; Kirmaier, C.; Ogilvie, J. P. Primary processes in the bacterial reaction center probed by two-dimensional electronic spectroscopy. *Proceedings of the National Academy of Sciences* **2018**,
- [21] Bukartė, E.; Paleček, D.; Edlund, P.; Westenhoff, S.; Zigmantas, D. Dynamic band-shift signal in two-dimensional electronic spectroscopy: A case of bacterial reaction center. *The Journal of Chemical Physics* **2021**, *154*, 115102.
- [22] Higgins, J. S.; Dardia, A. R.; Ndife, C. J.; Lloyd, L. T.; Bain, E. M.; Engel, G. S. Leveraging Dynamical Symmetries in Two-Dimensional Electronic Spectra to Extract Population Transfer Pathways. *The Journal of Physical Chemistry A* *0*, null.

- [23] Witkowski, A.; Moffitt, W. Electronic Spectra of Dimers: Derivation of the Fundamental Vibronic Equation. *The Journal of Chemical Physics* **1960**, *33*, 872–875.
- [24] Fulton, R. L.; Gouterman, M. Vibronic Coupling. I. Mathematical Treatment for Two Electronic States. *The Journal of Chemical Physics* **1961**, *35*, 1059–1071.
- [25] Förster, T. *Modern Quantum Chemistry, edited by O. Sinanoglu*; Academic Press Inc., New York. (1996), p 93.
- [26] Seibt, J.; Pullerits, T. Beating Signals in 2D Spectroscopy: Electronic or Nuclear Coherences? Application to a Quantum Dot Model System. *The Journal of Physical Chemistry C* **2013**, *117*, 18728–18737.
- [27] Qian, W.; Jonas, D. M. Role of cyclic sets of transition dipoles in the pump–probe polarization anisotropy: Application to square symmetric molecules and perpendicular chromophore pairs. *The Journal of Chemical Physics* **2003**, *119*, 1611–1622.
- [28] Tiwari, V.; Peters, W. K.; Jonas, D. M. Electronic resonance with anticorrelated pigment vibrations drives photosynthetic energy transfer outside the adiabatic framework. *PNAS* **2013**, *110*, 1203–1208.
- [29] Ryu, I. S.; Dong, H.; Fleming, G. R. Role of Electronic-Vibrational Mixing in Enhancing Vibrational Coherences in the Ground Electronic States of Photosynthetic Bacterial Reaction Center. *The Journal of Physical Chemistry B* **2014**, *118*, 1381–1388.
- [30] Tiwari, V. Non-adiabatic Mechanism for Photosynthetic Energy Transfer and All-Optical Determination of Concentration Using Femtosecond Lasers. *Ph.D. Thesis, University of Colorado, Boulder*. **2014**,
- [31] Farrow, D. A.; Smith, E. R.; Qian, W.; Jonas, D. M. The polarization anisotropy of vibrational quantum beats in resonant pump- probe experiments : Diagrammatic calculations for square symmetric molecules The polarization anisotropy of vibrational quantum beats in resonant pump-probe experiments : Diagramma. **2008**, *174509*.
- [32] Jonas, D. M.; Lang, M. J.; Nagasawa, Y.; Joo, T.; Fleming, G. R. Pump-Probe Polarization Anisotropy Study of Femtosecond Energy Transfer within the Photosynthetic Reaction Center of Rhodobacter sphaeroides R26. *The Journal of Physical Chemistry* **1996**, *100*, 12660–12673.
- [33] Tiwari, V.; Peters, W. K.; Jonas, D. M. Electronic energy transfer through non-adiabatic vibrational-electronic resonance. I. Theory for a dimer. *The Journal of Chemical Physics* **2017**, *147*, 154308.
- [34] Peters, W. K.; Tiwari, V.; Jonas, D. M. Nodeless vibrational amplitudes and quantum nonadiabatic dynamics in the nested funnel for a pseudo Jahn-Teller molecule or homodimer. *The Journal of Chemical Physics* **2017**, *147*, 194306.

- [35] Tiwari, V.; Jonas, D. M. Electronic energy transfer through non-adiabatic vibrational-electronic resonance. II. 1D spectra for a dimer. *The Journal of Chemical Physics* **2018**, *148*, 84308.
- [36] Rancova, O.; Jankowiak, R.; Kell, A.; Jassas, M.; Abramavicius, D. Band Structure of the Rhodobacter sphaeroides Photosynthetic Reaction Center from Low-Temperature Absorption and Hole-Burned Spectra. *The Journal of Physical Chemistry B* **2016**, *120*, 5601–5616.
- [37] Jordanides, X. J.; Scholes, G. D.; Fleming, G. R. The Mechanism of Energy Transfer in the Bacterial Photosynthetic Reaction Center. *The Journal of Physical Chemistry B* **2001**, *105*, 1652–1669.